Environmental Science & Technology

pubs.acs.org/est

Article

Studying Microplastic Incorporation into Corals Using CARS

Tomoko Takahashi,* Cecilia D'angelo, Jacob Kleboe, Joerg Wiedenmann, Gavin L. Foster, and Sumeet Mahajan

Cite This: *Environ. Sci. Technol.* 2026, 60, 3438−3448

Read Online

ACCESS | Metrics & More | Article Recommendations | Supporting Information

ABSTRACT: Microplastic pollution is a serious threat to marine organisms, including reef-building corals. Corals are known to incorporate microplastics, which could potentially provide an archive of information to trace present and past microplastic pollution. In this study, a label-free chemical analytical method for rapid visualization of microplastics incorporated in coral tissue and skeletons is proposed by using a coherent anti-Stokes Raman scattering (CARS) microscope combined with two-photon excited fluorescence (TPEF) detection. *Acropora polystoma* was maintained in an environment with a high concentration of polyethylene (PE) beads ranging from 0.7 to 5 μm in size. PE beads were successfully visualized, and the number of incorporated beads per skeleton area was quantitatively analyzed using the proposed technique. Notably, plastic beads were only found in the skeleton of coral colonies showing signs of localized tissue loss. Further CARS analysis of tissue found that a number of microplastics were trapped in the areas where tissue loss was observed due to bleaching or physical tissue removal, whereas minimal amounts were observed within healthy tissue. These results suggest that unhealthy conditions which lead to tissue loss and bleaching may accelerate microplastic incorporation into coral tissue and further into skeletons. Our study shows the ability of our CARS-based method to help understand how microplastics are incorporated into corals and will lead to improved tracking of their accumulation in coral reefs.

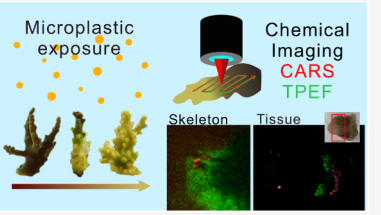

KEYWORDS: *microplastics, coherent anti-stokes raman scattering (CARS), coral, bleaching, label-free analysis*

INTRODUCTION

In recent years, plastic pollution of marine environments has become a global issue. Once plastics enter the ocean, they are transported throughout the ocean system and are considered to persist in the environment for decades.[1] In particular, microplastics with sizes less than 5 mm[1−3] are detected not only in water and sediments but also in bodies of large- to small-scale marine organisms.[4−13] Negative biological impacts related to microplastics have now been reported through laboratory-based studies for many different types of organisms. Examples include fundamental processes (e.g., development, reproduction) of benthic animals such as mussels and lugworms[14] and the feeding capability of copepods.[15] As microplastic impacts are different among species and also depend on concentrations and other conditions, detailed species-to-species investigations are still needed to fully understand and quantify the biological impacts of microplastic pollution.

Reef-building corals are not an exception, and microplastics have been found in the tissue and skeletons of natural corals.[16,17] It is thought that corals can incorporate microplastics into their skeletal matrix through intake mechanisms such as ingestion.[18−20] This offers the intriguing possibility of using the coral skeleton as an archive of marine plastic pollution, to which the coral and, by extension, the reef have been exposed.

In a laboratory setting, fluorescent-labeled or easily recognizable microplastics are often used to investigate the incorporation mechanism of microplastics in corals. While in the natural environment a large number of microplastics are not colored or labeled, the use of fluorescent beads has led to insights into the interaction of microplastics with corals in laboratory environments. Ingestion and egestion of microplastic particles have been observed in a wide variety of coral species.[19,21−23] Negative health effects have also been recorded in certain coral species exposed to high concentrations of microplastics.[24] In particular, Reichert et al. (2018) found that, after incubation of corals in a tank with 0.1 g/L of PE particles (37−163 μm), areas where tissue necrosis and bleaching were observed contained higher concentrations of plastic adhesion in these regions.[21] It was also reported that bleached coral polyps incorporate more microplastics in their tentacles and tissue, and smaller particles remained for longer periods within the coral tissue in comparison to larger particles; this is within a comparison of microplastics with sizes of 3, 6, and 11 μm.[25,26] Microplastics were eventually expelled during the experiments performed in the work of Okubo et al.[26]

Received: August 3, 2025
Revised: January 6, 2026
Accepted: January 8, 2026
Published: January 22, 2026

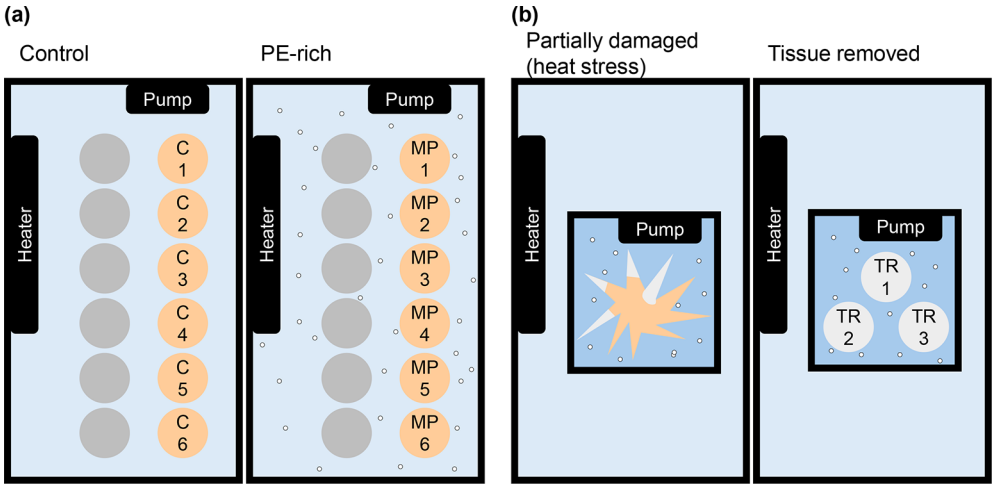

Figure 1. Schematic diagrams of the tanks used in (a) Experiment 1 and (b) Experiment 2. In Experiment 1, six coral pieces were placed in each tank, labeled as C1−C6 for the control tank and MP1−MP6 for the PE-rich tank. In Experiment 2, one tank contained a coral colony with some fragments partially damaged by exposure to hot water, and another tank contained three coral pieces with tissue manually removed using a water flosser (labeled as TR1−TR3). The gray area shown in (a) indicates the presence of other coral samples of different species in the tanks that were not used in this study and were grown for other studies.

For environmental samples, colored or fibrous plastics can be visually identified in the skeleton based on their distinctive features, with the year in which they are trapped estimated from coral growth band analysis. In the study of Krishnakumar et al.,[27] the plastics were visually found in the coral skeleton by microscopic observation and then confirmed by Fourier transform infrared (FT-IR) spectroscopy. However, the visualization of less distinctive generic plastics, which are more commonly seen in natural environments, is an important direction in microplastic studies, and label-free analytical methods are required for this. Ideally, such label-free chemical analytical techniques would be combined with microscopy and have the potential to visualize microplastics in coral skeletons on a submicron scale. Incorporated polyethylene terephthalate (PET) beads in the skeleton have been successfully visualized via scanning electron microscopy with energy-dispersive X-ray spectroscopy (SEM-EDX) quantifying elemental compositions.[20] However, SEM-EDX is only effective for plastics with distinctive elemental compositions and not applicable to the detection of polypropylene (PP) and polyethylene (PE), which comprise only carbon (C) and hydrogen (H), yet represent the most common types of plastics found in aquatic environments.[1] FT-IR spectroscopy and Raman spectroscopy, which are commonly used for identification of microplastic materials based on the molecular characteristics, can fundamentally differentiate between common C- and H-based polymers, such as PE, PP, and polystyrene (PS). Proof-of-concept studies using these techniques have been demonstrated to establish methods to localize microplastics in biological samples.[28] While these techniques have the potential to detect microplastic fragments in coral skeletons,[29−31] these require long measurement times, typically several seconds per spectral acquisition, which makes them impractical to scan a large area of coral skeletons to visualize generic microplastics. Therefore, the current standard approach for quantifying the incorporated microplastics within coral skeletons uses destructive techniques that dissolve the skeleton and extract the microplastic material,[16,32] which allows analysis of a large volume of samples but loses spatial information relating to the location within the skeleton where the plastics are accumulating. For a comprehensive analysis of how microplastics are incorporated into the skeletal matrix and also to develop a coral-based archive of microplastic pollution spreading in natural environments, a label-free, nondestructive, rapid analytical method is required.

Coherent anti-Stokes Raman scattering (CARS) microscopy, a label-free, nondestructive molecular analysis technique, is a promising technique for the visualization of microplastic distribution in a sample. Compared to the weak spontaneous Raman signal, whose intensity is one in ten million of the irradiating laser power, the CARS signal is significantly strong due to the vibrational coherence generated by the irradiating pump and Stokes laser beams, whose wavelength difference matches the frequency of the target's molecular vibration.[33] Its submicron spatial resolution[34] is significantly better than FT-IR spectroscopy, which is typically ∼20 μm, because CARS uses a laser with a shorter wavelength for excitation.[35,36] This also enables CARS to directly measure water-submerged samples, which FT-IR is not capable of analyzing due to the strong absorption of IR light by water. In addition, CARS images are free from the background signal due to fluorescence, whereas Raman spectroscopy often suffers from a strong fluorescence background emitted by bio-organic matter, additives, or pigments of microplastics.[37] Two-photon excited fluorescence (TPEF) signals can be taken simultaneously and separately in different channels, making it a multimodal technique. The technique has been used extensively for in vivo imaging of biomedical samples, in particular live cells.[38−40] Rapid three-dimensional chemical imaging is also possible for samples with a thickness within the penetration depth of near-infrared laser beams used for CARS.[41,42] CARS has additionally been recently applied to corals in the case of imaging the distribution of skeletal organic molecules across a section of coral skeleton with a theoretical resolution of <500 nm.[34] CARS and related techniques have been applied to the identification[43] and detection of different microplastics, including PE and PS, and in-flow classification of microplastics and algae[44] and the detection of PS beads attached to plankton.[45]

https://doi.org/10.1021/acs.est.5c10668
Environ. Sci. Technol. 2026, 60, 3438−3448

In this work, a label-free direct measurement method for microplastic visualization in coral tissue and skeletons by three-dimensional multimodal CARS and TPEF laser scanning microscopy is proposed. The method is first applied to the skeleton of samples of *Acropora polystoma* maintained in a microplastic-rich environment. This work will focus on the demonstration of our novel analytical method to visualize the incorporation of unlabeled microplastics in coral bodies and further discuss the responses of the corals with tissue loss to microplastic exposure.

MATERIALS AND METHODS

Plastics and Corals

Clear PE beads with a size range of 0.7−5 μm (PENS-0.98 740−4990 nm, Cospheric) were used in this study. These clear beads were specifically chosen for this study because they are unlabeled and comprised solely of C and H, representing a common type of polymer whose identification is fundamentally challenging for elemental-based analysis methods. *A. polystoma* (unconfirmed origin, purchased via the British aquaristic trade in the UK in 2008), a hard coral species, was selected for the microplastic exposure experiment conducted in this study as fast skeleton growth was expected.[46] *A. polystoma* had been cultured and propagated by fragmentation in the experimental mesocosm of the Coral Reef Laboratory of the University of Southampton.[47]

For the validation of the proposed method, a skeleton fragment with PE beads on its surface was prepared. PE beads suspended in ethanol were dropped on a skeleton fragment of *A. polystoma* and allowed to dry before imaging, leaving the microplastics attached to the surface.

Microplastic Exposure of Corals

Two experiments with different exposure periods of microplastics were performed. The longer experiment (hereafter referred to as Experiment 1) was performed across a two-week period to analyze microplastic incorporation into the skeleton, whereas the shorter experiment (hereafter referred to as Experiment 2) was performed for 1 week to analyze microplastic incorporation into the tissue. The schematic of the setup of the tanks for Experiments 1 and 2 is shown in Figure 1(a) and (b), respectively. During Experiment 1, two experimental tanks that were filled with 35 L of artificial seawater with salt dissolved in the water were split from the mesocosm system. The artificial seawater used for the experiments conducted in this study was taken from the mesocosm system. Details of the water quality control are described elsewhere.[47,48] The maintenance of corals and control of environmental parameters were carried out as per protocols described previously.[48,49] A period of 7 days was given for tank stabilization prior to the experiment start. 0.525 g of the PE beads was added to one tank (hereafter referred to as the PE-rich tank), i.e., the PE concentration in the PE-rich tank was approximately 15 mg/L. This concentration was chosen to match the range of μm-sized microplastic exposures to marine organisms used in previous studies.[50,51] No plastics were added to the other tank (hereafter referred to as the control tank). In both tanks, a pump was attached to circulate the water and PE beads for the PE-rich tank. Six pieces of healthy *A. polystoma* were placed in each tank with the same configuration and were kept for up to 14 days (C1−C6 in the control tank, MP1−MP6 in the PE-rich tank). Two liters of artificial seawater (for the PE-rich tank, 2 L of artificial seawater with PE beads of 30 mg, with a concentration of 15 mg/L PE beads) were changed three times per week to maintain the water quality. The salinity and temperature were kept in the range of 32−34‰ and 26.0−26.5 °C, respectively.

Since a difference between corals with and without tissue loss (i.e., obvious color change from brown to white) was seen during Experiment 1 (details discussed in the Results and Discussion section), Experiment 2 was conducted to further investigate the impact of tissue loss on microplastic incorporation. Two tanks with a pump each filled with 2.5 L of artificial seawater and 37.5 mg of PE beads (i.e., 15 mg/L PE beads) were prepared for Experiment 2. The tanks were set in a large water bath maintained at the same water temperature range as Experiment 1. In one tank, a coral colony with some artificially stressed tissue was placed. The stress response was produced by placing them into 80 °C hot water for 10 s prior to Experiment 2 so that the tissue was partially damaged. Tissue loss did not occur immediately after the heat stress treatment and gradually appeared in some areas during the first couple of days of the experiment. In the other tank, three fragments with tissue removed manually using a water flosser were placed (labeled as TR1−TR3). For both tanks, the whole 2.5 L seawater was changed every day with the artificial seawater with a concentration of 15 mg/L PE beads to maintain the water quality.

Sample Preparation

After exposure to microplastics, all coral samples were transferred from the tanks to the laboratory. The samples from Experiment 1 were frozen at −24 °C for later analysis. Tissue of the samples from Experiment 2 was measured on the same day of the recovery, except for one sample where large-area mapping was performed 24 h after recovery (kept at 5 °C for one night). Samples from Experiment 1 had the peripheral part of each frozen coral sample cut and immersed in 0.5% sodium hypochlorite for one night. As a preliminary observation indicated tissue remained after this treatment, the fragments were further immersed in 2% of the same bleaching liquid for two nights. For some samples where remaining tissue was still seen, the fragments were then further immersed in 5% of the same bleaching liquid for 5 min. Following these treatments, all samples were immersed in purified water for at least one night. To measure the areas that are expected to be newly grown, the tips and nubbins were cut using a scalpel. The fragments were then cleaned using an ultrasonic bath for more than 30 s just before measurements to further ensure the removal of tissue and microplastic particles attached to the skeleton surface or passively lodged in skeletal pores, thereby ensuring that microplastics detected were embedded in the skeleton. To check whether PE beads were removed from the skeletal surface and pores by the procedure, an *A. polystoma* skeleton fragment that was kept in PE-rich water with a concentration of 15 mg/L for 3 nights was measured by the same protocol as for CARS and TPEF measurements, and no PE beads were found in the skeleton fragment. The details are described in Supporting Information. The samples from Experiment 2 also had the peripheral part cut and quickly washed with artificial seawater, then their tissue was measured without chemical bleaching or cleaning processes. After the tissue analysis, all samples from Experiment 2 were chemically bleached with the same process as the samples from Experiment 1. The surface of the samples was measured directly after the preparation protocol described in

https://doi.org/10.1021/acs.est.5c10668
Environ. Sci. Technol. 2026, 60, 3438−3448

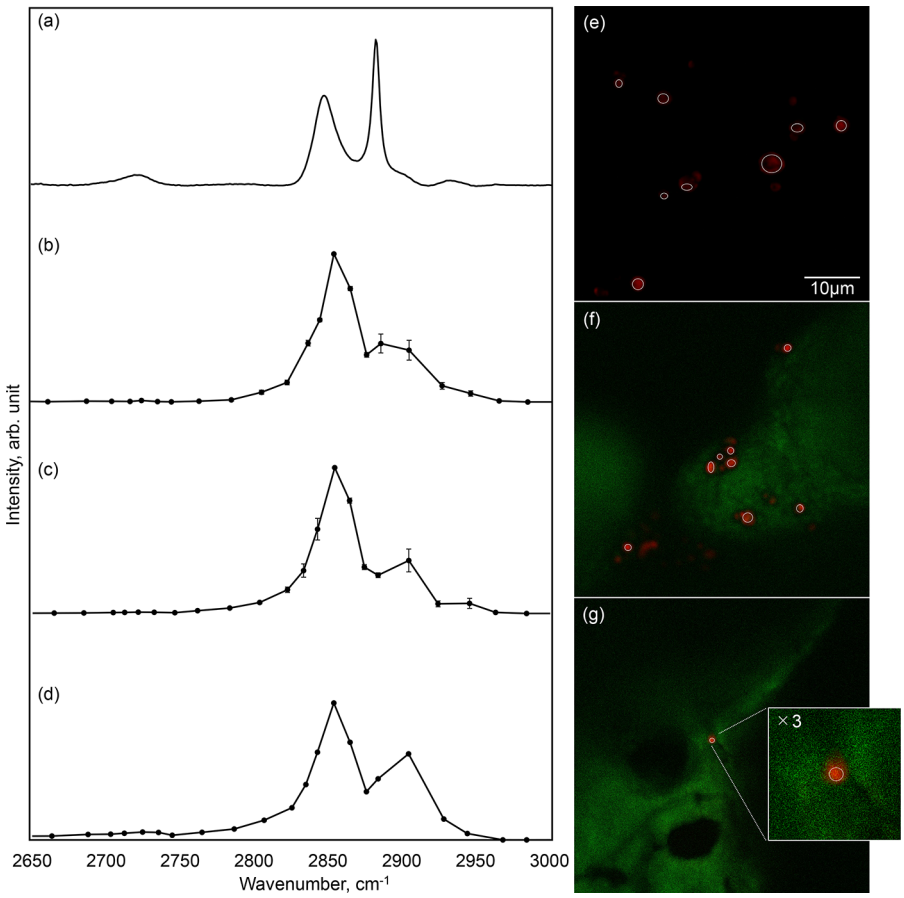

Figure 2. (a) Raman spectrum taken for a PE bead on a glass slide. (b–d) CARS spectrum taken for PE beads on a glass slide, on a coral skeleton, and detected in the skeleton of MP1, respectively. (e–g) Images of CARS signals of 2845 cm^{-1} shown in red, superimposed by TPEF signals shown in green, taken for (b–d), respectively. The enlarged image (3× magnification) is also shown in (g). The circles indicate the particles used for the calculation of the spectral intensity.

this section without prior sectioning, as it typically requires embedding a sample into plastic resin[34] which could compromise our ability to detect microplastic beads.

CARS Setup

A custom-built CARS system based on a fiber laser (picoEmerald, APE) and a laser scanning microscope (LSM 980, Zeiss) was used in this study. The Stokes beam (1031.5 nm) and pump beam (700–1300 nm) were spatially and temporally combined to generate the CARS signal. Simultaneously, TPEF signals were collected in the nondescanned detection mode. A 20× water-immersion objective (NA = 1) was used to image the samples directly in water or artificial seawater. Detailed specifications of the optical setup and the schematic diagram are provided in the (Supporting Information Figure S1).

The setup of Raman spectroscopy used to acquire a spectrum of a PE bead is described in the Supporting Information.

PE Bead Detection

In the Raman spectrum of a PE bead used in this study shown in Figure 2(a), the peaks seen around 2850 cm^{-1} and 2880 cm^{-1} are attributed to the CH_2 symmetric and asymmetric stretching modes[52] of PE, respectively. The CARS spectra of PE beads on a glass slide and a chemically bleached skeleton were produced by measuring the average intensity of individual microplastic particles for each wavenumber, as shown in Figure 2(b,c), respectively. The intensity of eight particles (marked with the circles in Figure 2(e,f)) was measured within the field of view (FOV), and for each particle, the CARS intensity was measured after subtracting the intensity of a dark image (pump beam only) to isolate only CARS-related signals. The same peaks seen in the Raman spectrum are observed in the CARS spectra, while the peak at ∼2880 cm^{-1} is larger than at ∼2850 cm^{-1} in CARS, which contrasts with Raman. This is considered to be because the peak at ∼2880 cm^{-1} is narrow, and the wavenumber resolution of the CARS system, 10–20 cm^{-1} in this study, was not enough to adequately resolve the peak. TPEF signals are barely seen in Figure 2(e), whereas the skeleton area is highlighted in the TPEF in Figure 2(f). This is because the *A. polystoma* skeleton is known to emit fluorescence (e.g., excitation wavelength of 397 nm and emission wavelength of 500 nm for bleached *A. polystoma*[53]). In our setup, this was collected with two-photon excitation using a band-pass filter of 520 ± 40 nm. As seen in Figure 2(c), the CARS spectrum of PE beads detected on the *A. polystoma* skeleton follows the trend of the spectrum of isolated PE beads.

Based on the CARS spectra obtained for the PE beads, the protocol to find PE beads in the coral samples was defined as follows:

- A large area was first scanned in the XY direction with a step size of approximately 0.4 μm (covering 424.27 μm in 1024 pixels) by tuning the beams for the detection of

https://doi.org/10.1021/acs.est.5c10668
Environ. Sci. Technol. 2026, 60, 3438–3448

the CARS signal at a wavenumber of 2845 cm^{-1} (peak) to search and visualize PE beads incorporated in tissue and skeletons efficiently. The pixel dwell time was set to 0.8 μs × 1 shot, taking two images with and without the Stokes beam, which results in <2 s to take one image.

- When a bright spot with a round shape or an aggregate of round shapes was found, the spot was scanned in the XY direction with a smaller step size of approximately 0.2 μm (covering 424.27 μm in 2048 pixels) targeting the same wavenumber. The pixel dwell time was set to 0.5 μs × 2 shots to enhance the signal-to-noise ratio, taking two images with and without the Stokes beam, which results in 10 s to take one image.
- A CARS image of 3005 cm^{-1} (no signal from PE) was taken at the same spot in the XY direction with a step size of approximately 0.2 μm (covering 424.27 μm in 2048 pixels) for microplastic verification. The pixel dwell time was set to 0.5 μs × 2 shots, taking two images with and without the Stokes beam, which results in 10 s to take one image.

2845 cm^{-1} was used for searching PE beads, as 2850 cm^{-1} might cause saturation of the intensity. When a round object was detected at only 2845 cm^{-1}, it was counted as a PE bead. With this protocol, the detection of particles larger than 1 μm in size in the skeleton was targeted (corresponding to approximately 2.5 and 5 pixels in the first and second scans, respectively). It should be noted that this protocol was defined for rapid PE detection. For the detection of other plastic types, we would need multiple acquisitions targeted at more wavenumber peak locations.[54] For validation, the spectrum shown in Figure 2(d) was taken for a round object in the skeleton of sample "MP1" found by following the protocol, as shown in Figure 2(g). Although the peak location at 2880 cm^{-1} is slightly shifted, the spectrum follows the trend of the PE beads. Therefore, it can be said that the PE beads incorporated in the skeleton are detectable by the proposed sample preparation method and protocol. To quantify the number density of PE beads per area, the skeletal area was calculated using TPEF signals. The detailed image processing method and the calculation procedure are described in the Supporting Information.

For PE bead detection in the tissue, areas where microplastics were observed were easily found, as a significant number of beads were seen. Therefore, a large area scan was not performed, and 2845 and 3005 cm^{-1} CARS images were acquired for the same FOV in the XY direction with a step size of approximately 0.4 μm (covering 424.27 μm in 1024 pixels). The pixel dwell time was set to the same as that of the large skeletal scan. The calculation method of the number of particles in tissue is described in Supporting Information.

RESULTS AND DISCUSSION

Coral Response to Microplastics during Experiment 1

Figure 3 shows images of the coral samples during Experiment 1. While all corals had brown tissue on the surface on Day 0, as shown in Figure 3, pronounced tissue loss was visually observed for MP1, MP5, and C5 by Day 11. Since MP5 and C5 were located at the same position within the tanks, this may be because of unfavorable local conditions in that area. This localized effect occurred despite consistent water circulation by a pump and regular water changes aimed at maintaining water quality. As no more growth was expected for the corals with

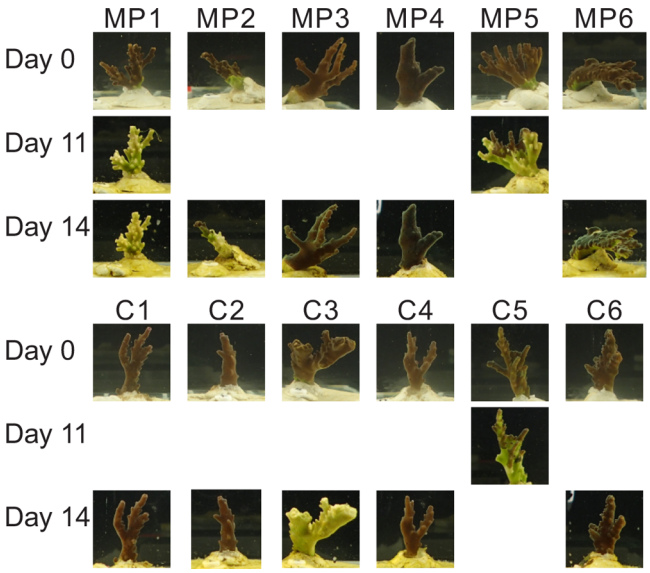

Figure 3. Photos of coral samples taken on Day 0, Day 11 (only for MP1, MP5, and C5), and Day 14. The photos of MP5 and C5 were not taken on Day 14, as they were recovered on Day 11.

massive tissue loss, MP5 and C5 were recovered on Day 11. While MP1 also showed the areas of bare skeleton without tissue, it was kept in the tank as a counterpart of C1 that remained healthy on Day 11. By Day 14, a large part of MP2 and C3 also lost tissue. A bare skeleton area was also observed on the bottom side of MP6. All samples were recovered on Day 14. As tissue loss occurred for samples both in the PE-rich and control tanks, it is considered that the observed tissue loss was not an impact of the PE beads used in this study.

Measurements of Skeletons

Table 1 shows the number of PE beads detected in *A. polystoma* skeletons for Experiment 1. As shown in Table 1, PE

Table 1. Number of PE Beads Detected in the Skeletons[a]

Label	PE (#)	Area (mm^2)	n (#/mm^2)	Label	PE (#)	Area (mm^2)	n (#/mm^2)
MP1	2	12.2	0.164	C1	0	13.5	0
MP2	9[b]	15.6	0.577	C2	0	14.5	0
MP3	0	13.5	0	C3	0	14.7	0
MP4	0	15.7	0	C4	0	11.5	0
MP5	8[c]	11.6	0.690	C5	0	10.9	0
MP6	3	20.0	0.150	C6	0	11.0	0

[a]"Area" indicates the scanned area calculated from TPEF images. [b]6 found in the same location. [c]2 aggregated.

beads were only found in a selection of the samples kept in the PE-rich condition, although all samples of MP1−MP6 and C1−C6 were scanned with an area of >10 mm^2 following the proposed protocol. MP2, at 9 beads detected, had the largest number of PE beads in the skeleton, and MP5 followed with 8 PE beads found in the skeleton. MP6 and MP1 had a relatively small number of PE beads, 3 and 2, respectively, whereas no PE beads were found in MP3 and MP4. No PE beads were found in the skeletons of control samples, which validates the reliability of microplastic detection using the proposed method. Figure 4 shows the PE beads detected in the CARS image for 2845 cm^{-1}, shown in red, within the *A. polystoma* skeletons, which are colored green (TPEF). The images are

https://doi.org/10.1021/acs.est.5c10668
Environ. Sci. Technol. 2026, 60, 3438−3448

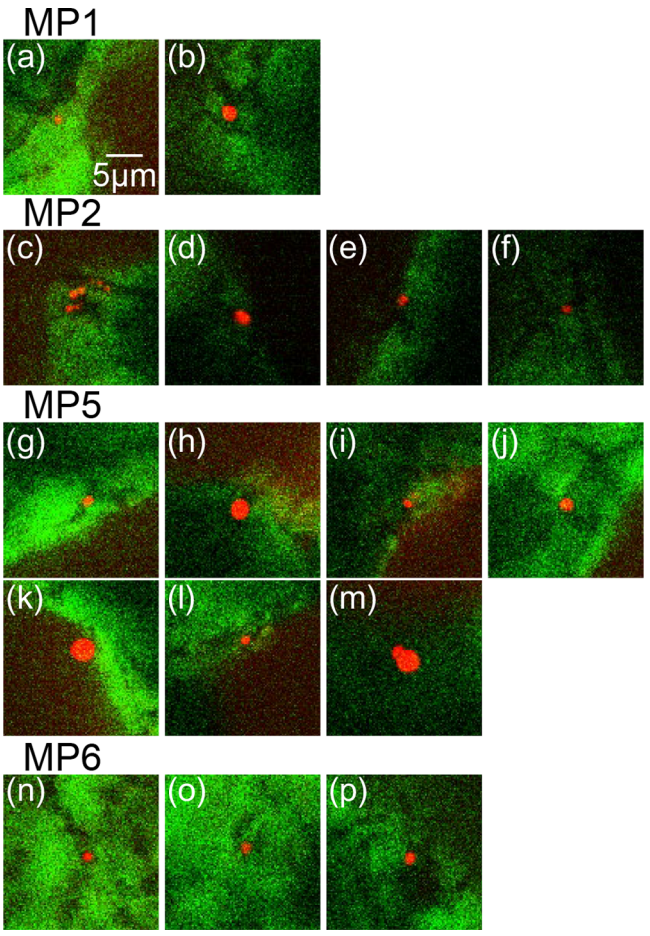

Figure 4. Images of the PE beads detected in the skeleton. The CARS image for 2845 cm^{-1} shown in red and the TPEF image shown in green are superimposed.

enlarged views, and the images with the original FOV are shown in Figure S3. All PE beads detected within the skeleton had sizes of approximately 1−3 μm, which were manually measured from the images. A cluster of 6 PE beads was observed at the same location for MP2, as shown in Figure 4(c), and 2 were detected as aggregates for MP5, as shown in Figure 4(m). It should be noted that no PE beads were visually seen in the bright-field images taken using the same objective. As the z-stack images were taken, the cross-sectional views of the PE beads detected in the skeleton were generated, as shown in Figure 5. The cross sections for all PE beads are shown in Figure S4. It can be seen from Figure 5 and Figure S4

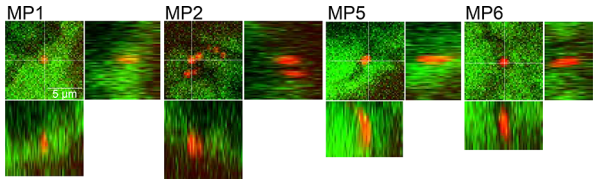

Figure 5. Examples of cross-sectional views of the PE beads detected in the skeleton. The central panel for each image set shows the XY image with overlaid dotted lines indicating the cross-section positions. The right panel displays the YZ cross-section, and the bottom panel shows the XZ cross-section for each image set. The CARS image for 2845 cm^{-1} shown in red and the TPEF image shown in green are superimposed.

that all PE beads were detected close to the skeleton edge, and all were buried in the skeleton, and some of them were covered with a thin skeleton layer with a thickness of several μm. This likely corresponds to the area of new growth during the experiment period, considering the growth rate of *A. polystoma*, which is expected to be a submillimeter increase for a two-week growth period.[55]

The analysis of the coral skeletons yielded two key findings concerning microplastic incorporation. From a technical standpoint, the proposed CARS and TPEF technique successfully demonstrated the rapid visualization of label-free microplastics incorporated into coral skeletons. The technique has a great advantage in finding μm-sized microplastics in a large skeletal area. With the proposed method, the acquisition time was only 0.8−1 μs per pixel for simultaneous acquisition of CARS and TPEF signals, which took less than 2 s per image of 1024 × 1024 pixels. This is extremely fast compared to FT-IR and Raman spectroscopy, which typically require several seconds per pixel. It should be noted, however, that a typical CARS system, such as the one used in this study, can acquire a CARS signal at only one wavenumber per scan. While PE beads were successfully detected by comparing the intensity at two wavenumbers in this work, identification of plastic fragments with complex shapes or different polymer types in natural environments would require multiple acquisitions targeting more peak locations, or ideally a full spectrum. Although scanning over all wavenumbers of interest takes more time, recent advances in hyperspectral CARS have demonstrated that a full spectrum can be acquired at speeds comparable to, or even faster than, those of conventional CARS systems.[56,57] While in this study we have demonstrated the application of CARS for rapid MP detection as a proof of concept, with further development, by integrating the proposed method with hyperspectral CARS technology, full-spectral CARS imaging can be readily realized, achieving scanning speeds that are fundamentally beyond the reach of FT-IR or spontaneous Raman spectroscopy. In addition, toward the direction of applications of the CARS and TPEF techniques to environmental samples, the sensitivity of signal quality depending on various factors such as morphology, aging, and weathering effects that are common problems in Raman spectroscopy analysis of microplastics needs to be investigated. For irregular shapes and samples with a rough surface, a part of a sample might be shown in the image,[44] and sectioning is required to fully capture the shape of plastic fragments, while detection should still be possible without sectioning the sample. It has been reported that molecular characteristic changes due to aging and weathering alter Raman spectral features such as intensity changes,[58,59] which should also affect CARS signals, and these should be investigated in future studies. Among common problems in Raman spectroscopy analysis of microplastics, the proposed technique will be powerful against the influences of pigments and attached organic matter that often cause a strong fluorescence background.

The results also revealed an interesting biological pattern regarding microplastic incorporation. Although the unintended tissue damage limited the ability to definitively evaluate the toxicological effects of microplastics on coral health, the results indicate that tissue loss and the amount of microplastics incorporated in corals are related. PE beads were found only in the skeletons of the samples MP1, MP2, MP5, and MP6, where bare skeleton areas were visually observed, but no PE

https://doi.org/10.1021/acs.est.5c10668
Environ. Sci. Technol. 2026, 60, 3438−3448

beads were found in the skeletons of the samples MP3 and MP4, where no obvious tissue loss was seen. While the impact of microplastics on tissue loss is unclear in this study, microplastics were detected specifically in coral fragments with bare skeletons due to tissue loss. This will be explored more in the following section, where *A. polystoma* tissue under different tissue necrosis treatments was further analyzed.

Measurements of Coral Tissue

From the analysis of the samples for Experiment 1, the visualization of microplastics in the coral skeletons was successfully demonstrated. In addition, it was found that microplastics were detected only in the skeletons of the samples characterized by bare skeleton areas devoid of any tissue, while tissue areas of the same coral were not examined for Experiment 1. As microplastics should be first incorporated into tissue and then further into the skeleton, to enable this investigation, the visualization of microplastics in the coral tissue was also demonstrated using the proposed CARS and TPEF technique. Experiment 2, where the coral colony was artificially bleached by heat stress or its tissue was mechanically removed, was additionally performed to investigate microplastic incorporation into tissue and to explore whether the associated tissue loss condition enhanced microplastic incorporation. Extracted fragments for CARS analysis from the colony samples grown during Experiment 2 are shown in Figure S5. The fragments dipped into hot water (labeled HS1, HS2, and HS3, which indicates "heat-stressed" fragments) got bleached, and the undipped portions remained healthy in the same sample, allowing direct comparison. Bleaching was assessed visually based on coral coloration, following the definition by Brown,[60] in which bleaching was characterized as whitening of corals due to loss of symbiotic algae and/or their pigments. The samples from which all tissue was removed using a water flosser are labeled TR1, TR2, and TR3, which indicates "tissue-removed" fragments. The control sample taken from the same colony for Experiment 2 has only healthy areas with no pretreatment.

At the boundary between bleached and unbleached regions, the boundary is clearly seen as dark (lower) and bright (upper) regions, as shown in Figure 6(d) (fluorescence bright-field image). In the bright region, the native green fluorescent protein (GFP) contained in the coral tissue is detected in the wavelength ranges of Figure 6(d).[61] A part of the healthy tissue is also seen as a bright region in Figure 6(c) (TPEF). Bright spots (a few μm in size) are densely observed exclusively within the bleached regions shown in Figure 6(a) (2845 cm^{-1} CARS). These spots are considered to be PE beads because they do not appear in 6(b) (3005 cm^{-1} CARS) or 6(c). Zooxanthellae, typically measuring 5−13 μm,[62] were visually observed in both bleached and unbleached regions in Figure 6(e), the bright-field image illuminated by a laser beam with a wavelength less sensitive to the tissue's chemicals. As zooxanthellae contain lipid that has strong Raman signals at both 2845 and 3005 cm^{-1},[63] they are also detected as bright spots in Figure 6(a,b). A video of the 3D sections of Figure 6 is shown in movie S1. Figure 7 shows typical CARS and TPEF images of (a,b) bleached and (c,d) healthy areas. Videos of three-dimensional sections of Figure 7(a−d) are shown in movies S2−S5, respectively. Two separate layers of zooxanthellae (shown in light red due to a mixture of 2845 and 3005 cm^{-1} CARS signals) and ectodermis (shown in green due to GFP signals) are seen in Figure 7(c,d). However, in Figure 7(a,b), zooxanthellae are spread randomly in the FOV, and ectodermis tissue is barely seen. The PE beads shown in red are detected only in Figure 7(a,b). There was no significant difference in the number of microplastics incorporated in the tissue between the treatments: heat stress or tissue removal using a water flosser. Table 2 shows the number of plastics found in the tissue for different treatment samples. As there were many particles detected in the tissue, unlike the skeleton, the measurement was performed for one FOV (424.27 × 424.27 μm) with a stack of 21 images (a 1 μm step). The size range of the particles in the tissue was set from 2 to 5 μm for reliable detection. The average diameters of detected particles were calculated from 2.2 to 2.7 μm, which is consistent with the average size of the PE beads used in this study. The detailed detection and calculation method of diameter are described in Supporting Information. It is clearly seen that PE beads are accumulated in the bare skeleton areas of both samples with heat stress and tissue removal treatment, whereas plastic accumulation was not observed in the healthy areas, even near the areas stressed by the hot water.

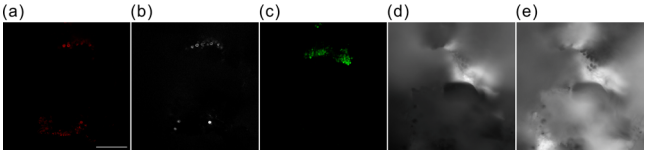

Figure 6. Images of the interface between bleached and unbleached areas taken for (a) 2845 cm^{-1} CARS, (b) 3005 cm^{-1} CARS, (c)TPEF, (d) fluorescent bright field (excitation at 488 nm, emission at 509 nm), and (e) fluorescence bright field (excitation at 353 nm, emission at 465 nm). The scale bar indicates 100 μm.

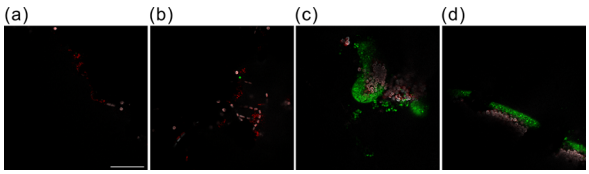

Figure 7. Examples of CARS and TPEF images of (a,b) bleached areas and (c,d) healthy areas. CARS and TPEF images are superimposed in red (2845 cm^{-1} CARS), white (3005 cm^{-1} CARS) and green (TPEF). Excitation and collection wavelengths for TPEF are the same as those in Figure 6. The scale bar indicates 100 μm.

Figure 8 shows a large-area, one-dimensional map of the number of plastic particles detected in the tissue of sample HS1. Measurements were performed along three lines on the x-axis, each separated by a distance sufficient to avoid overlap in the FOV. It should be noted that a slight misalignment of the CARS images taken at 2845 and 3005 cm^{-1} was seen in the healthy area imaged in line 2, possibly due to the movement of living tissue cells, as shown in Figure 8. For this image, the intensity of the detected particles (N = 3) in the CARS image acquired at 2845 cm^{-1} was manually compared with the corresponding regions in the CARS image taken at 3005 cm^{-1}, and all regions were determined not to be plastics as bright spots with a similar size were seen in the vicinity of the regions of detected particles at 2845 cm^{-1} in the CARS signals taken for 3005 cm^{-1}. For all three lines, plastic particles were found only in the bleached areas. No obvious relationship was observed between the distance and number of plastic particles

https://doi.org/10.1021/acs.est.5c10668
Environ. Sci. Technol. 2026, 60, 3438−3448

Table 2. Number of Plastics Found in Tissue[a]

		Heat stressed			Tissue removed			
		HS1	HS2	HS3	TR1	TR2	TR3	Cont.
Bleached	#	5	87	52	24	31	209	-
	diameter	2.4 ± 0.2	2.5 ± 0.5	2.4 ± 0.4	2.7 ± 0.7	2.5 ± 0.5	2.5 ± 0.5	-
	#	18	86	155	8	48	43	-
	diameter	2.2 ± 0.2	2.5 ± 0.4	2.5 ± 0.4	2.3 ± 0.2	2.5 ± 0.5	2.4 ± 0.3	-
	#	25	171	315	52	-	52	-
	diameter	2.4 ± 0.3	2.5 ± 0.4	2.5 ± 0.4	2.5 ± 0.4		2.5 ± 0.4	-
Healthy	#	0	0	0	-	-	-	0
	#	0	0	-	-	-	-	0
	#	0	0	-	-	-	-	0

[a]The unit of diameter is μm. The scanned area of 424.27 × 424.27 μm with a stack of 21 images (a 1 μm step) was taken for each.

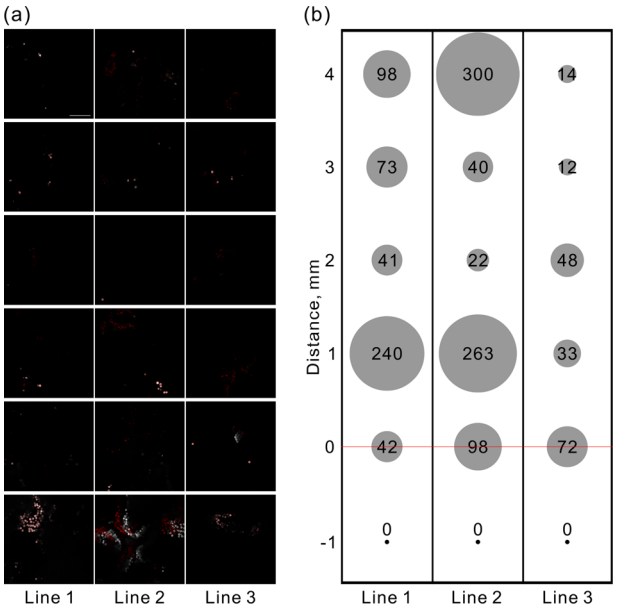

Figure 8. (a) Images taken according to the *y*-axis and (b) one-dimensional map of the number of plastic particles detected in the tissue of the HS1 sample (3 different lines). The scanned area of 424.27 × 424.27 μm with a stack of 51 images (a 1 μm step) were taken for each, except for the image sets taken at the distance = 0 where a stack of 101 images were taken as the location is a dynamic region with both healthy and bleached areas. The numbers of plastic particles at the distance = 0 were divided into 2. The distance = 0 is the location where both healthy and bleached areas were seen in one field of view, and the negative and positive directions of the *y*-axis indicate the distances from the location at the distance = 0 toward the healthy areas and bleached areas, respectively. CARS and TPEF images are superimposed in red (2845 cm^{-1} CARS), white (3005 cm^{-1} CARS), and green (TPEF). The scale bar in (a) indicates 100 μm.

detected in the tissue, while the plastics were spread out throughout the bleached areas.

These analyses clearly demonstrate that microplastic accumulation was exclusively observed in the coral tissue, exhibiting signs of bleaching or tissue loss. It can be assumed that healthy tissue does not accumulate microplastics, as it has an active cleaning function,[21] while bleached areas lose the function and accumulate floating matter in the water on the surface. It is also the case with the remaining damaged tissue after the treatment of tissue removal using a water flosser, considering that the samples with the treatment still accumulated microplastics. This observation supports the previous finding that bleached corals tend to incorporate more microplastics into their tissue than healthy corals[26] and we further observed incorporation into tissue and skeletons from CARS analysis. Considering a possible microplastic incorporation scenario suggested by Hierl et al. (2021),[20] some PE particles that became attached to the outer epidermis of the coral's tentacles were mistakenly ingested, then overgrown by the skeleton (aragonite), and finally encrusted. It should be noted, however, that although the skeletons of samples for Experiment 2 were also measured by following the proposed protocol, no plastics were identified in any samples. While the absence of plastics in the skeletons of TR1−TR3 is reasonable, as most tissue was manually removed using a water flosser prior to Experiment 2, this result is contradictory to the expectation derived from Experiment 1 for the HS1−HS3 samples, which retained tissue at the beginning of Experiment 2. This might be because bleaching occurred too quickly for sufficient skeletal growth to occur. While tissue was not immediately removed with the heat stress given to the samples of HS1−HS3, bleaching already started on Day 0. Then the expansion of bleached areas stopped by Day 3. There might have been, therefore, insufficient time for the skeleton to overgrow the plastics. Meanwhile, the level of tissue loss was gradually increasing over 2 weeks (11 days for MP5 and C5) during Experiment 1. It could be assumed that microplastic incorporation in the skeleton tends to occur frequently at compromised tissue, between the areas with and without healthy tissue, where microplastics are accumulated, yet the coral still retains the ability to incorporate materials into its body. When the speed of tissue loss is slow, such compromised tissue may have time to incorporate microplastics into their skeletons. This needs to be confirmed by further studies focusing on measuring the compromised areas of coral samples at different speeds at which tissue loss progresses. Continuous in vivo live monitoring of tissue loss propagation and microplastic incorporation in tissue will be effective for this, which will be performed in our future studies.

Coral bleaching from rising sea surface temperature and nutrient stress is one of the greatest threats facing corals in the modern ocean. While Isa et al. suggested that microplastics could exacerbate the effect of thermal stress on corals,[64] the environmental change could also potentially accelerate microplastic incorporation in corals and become an additional factor in the degradation of coral reefs. The proposed method, utilizing CARS and TPEF techniques, offers a label-free chemical analytical approach for the rapid visualization of microplastics incorporated into coral skeletons and tissue. The application of such rapid, label-free, and nondestructive

https://doi.org/10.1021/acs.est.5c10668
Environ. Sci. Technol. 2026, 60, 3438−3448

analytical techniques extends beyond the corals targeted in this study. Indeed, establishing these methods serves as a prerequisite for gaining deeper insights into the mechanisms of microplastic incorporation across diverse marine organisms, thereby advancing research on their ecological impacts. Specifically, regarding the findings of this research, by enabling fast detection of microplastics within corals, this technique could contribute to the monitoring of microplastic incorporation in natural corals in a drastically changing ocean environment, thereby contributing to the investigation of microplastic impacts on corals as well as tracking plastic pollution in the ocean, leveraging the intriguing possibility of using the coral skeleton as an archive of marine plastic pollution.

■ ASSOCIATED CONTENT

Supporting Information

The Supporting Information is available free of charge at https://pubs.acs.org/doi/10.1021/acs.est.5c10668.

Video of the three-dimensional section of Figure 6 (Movie S1) (AVI)
Video of the three-dimensional section of Figure 7(a) (Movie S2) (AVI)
Video of the three-dimensional section of Figure 7(b) (Movie S3) (AVI)
Video of the three-dimensional section of Figure 7(c) (Movie S4) (AVI)
Video of the three-dimensional section of Figure 7(d) (Movie S5) (AVI)
Details on the evaluation of removal procedures of attached microplastics, CARS setup, Raman spectroscopy setup, calculation of the scanned skeletal area, and calculation of the number of particles in tissue; schematic of the CARS setup (Figure S1); example image of the process for the skeletal area calculation (Figure S2); original and enlarged images of all PE beads detected in the skeletons (Figure S3); cross-sectional views of all PE beads detected in the skeleton (Figure S4); coral samples measured for tissue analysis (Figure S5); coral colonies before and after Experiment 2 (Figure S6) (PDF)

■ AUTHOR INFORMATION

Corresponding Author

Tomoko Takahashi − *Research Institute for Global Change, Japan Agency for Marine-Earth Science and Technology (JAMSTEC), Yokosuka, Kanagawa 2370061, Japan; Department of Chemistry and the Institute for Life Sciences, University of Southampton, Southampton SO17 1BJ, U.K.;* orcid.org/0000-0002-2916-7205; Email: takahas@jamstec.go.jp

Authors

Cecilia D'angelo − *Coral Reef Laboratory, School of Ocean and Earth Science, University of Southampton, Southampton SO14 3ZH, U.K.*

Jacob Kleboe − *Department of Chemistry and the Institute for Life Sciences, University of Southampton, Southampton SO17 1BJ, U.K.*

Joerg Wiedenmann − *Coral Reef Laboratory, School of Ocean and Earth Science, University of Southampton, Southampton SO14 3ZH, U.K.*

Gavin L. Foster − *School of Ocean and Earth Science, University of Southampton, Southampton SO14 3ZH, U.K.*

Sumeet Mahajan − *Department of Chemistry and the Institute for Life Sciences, University of Southampton, Southampton SO17 1BJ, U.K.;* orcid.org/0000-0001-8923-6666

Complete contact information is available at: https://pubs.acs.org/10.1021/acs.est.5c10668

Notes

The authors declare no competing financial interest.

■ ACKNOWLEDGMENTS

This work was supported by the Japan Society for the Promotion of Science (JSPS): Fostering Joint International Research (A) (Grant number: 20KK0336). This work was also partly supported by JSPS: Grant-in-Aid for Scientific Research (B) (Grant number: 21H01557), the Natural Environment Research Council (NERC) (Grant number: NE/T001364/1), the European Research Council Advanced Grant Micro-ns2Reefs (Grant number: 884650), and the Engineering and Physical Sciences Research Council (EPSRC) grant (Grant number: EP/T020997/1). The authors also acknowledge the funding support from the School of Chemistry & Chemical Engineering, the University of Southampton (Grant number: DTP EP/N509747/1). The authors thank Hannah Swadling, Ffion Smith, George Clarke, and Robbie Robinson for their great assistance in conducting the experiments. The authors also thank Dr. Yukiko Nagai, Dr. Takashi Toyofuku, and Dr. Tom Chalk for helping conduct the preliminary experiment.

■ REFERENCES

(1) Hidalgo-Ruz, V.; Gutow, L.; Thompson, R. C.; Thiel, M. Microplastics in the marine environment: A review of the methods used for identification and quantification. *Environ. Sci. Technol.* **2012**, *46*, 3060−3075.

(2) Jemec Kokalj, A.; Dolar, A.; Drobne, D.; Marinšek, M.; Dolenec, M.; Škrlep, L.; Strmljan, G.; Mušič, B.; Škapin, A. S. Environmental hazard of polypropylene microplastics from disposable medical masks: Acute toxicity towards Daphnia magna and current knowledge on other polypropylene microplastics. *Micropl. Nanopl.* **2022**, *2*, 1.

(3) Menzel, T.; Meides, N.; Mauel, A.; Mansfeld, U.; Kretschmer, W.; Kuhn, M.; Herzig, E. M.; Altstädt, V.; Strohriegl, P.; Senker, J.; et al. Degradation of low-density polyethylene to nanoplastic particles by accelerated weathering. *Sci. Total Environ.* **2022**, *826*, 154035.

(4) Wright, S. L.; Thompson, R. C.; Galloway, T. S. The physical impacts of microplastics on marine organisms; A review. *Environ. Pollut.* **2013**, *178*, 483−492.

(5) Guzzetti, E.; Sureda, A.; Tejada, S.; Faggio, C. Microplastic in marine organism: Environmental and toxicological effects. *Environ. Toxicol. Pharmacol.* **2018**, *64*, 164−171.

(6) Raju, P.; Santhanam, P.; Perumal, P.; et al. Impacts of microplastics on marine organisms: Present perspectives and the way forward. *Egypt. J. Aquat. Res.* **2022**, *48*, 205−209.

(7) Andrady, A. L. Microplastics in the marine environment. *Mar. Pollut. Bull.* **2011**, *62*, 1596−1605.

(8) Avio, C. G.; Gorbi, S.; Regoli, F. Plastics and microplastics in the oceans: From emerging pollutants to emerged threat. *Mar. Environ. Res.* **2017**, *128*, 2−11.

(9) Everaert, G.; Van Cauwenberghe, L.; De Rijcke, M.; Koelmans, A. A.; Mees, J.; Vandegehuchte, M.; Janssen, C. R. Risk assessment of microplastics in the ocean: Modelling approach and first conclusions. *Environ. Pollut.* **2018**, *242*, 1930−1938.

(10) Sharma, S.; Chatterjee, S. Microplastic pollution, a threat to marine ecosystem and human health: A short review. *Environ. Sci. Pollut. Res. Int.* **2017**, *24*, 21530−21547.

(11) Gunaalan, K.; Nielsen, T. G.; Rodríguez Torres, R.; Lorenz, C.; Vianello, A.; Andersen, C. A.; Vollertsen, J.; Almeda, R. Is zooplankton an entry point of microplastics into the marine food web? *Environ. Sci. Technol.* **2023**, *57*, 11643−11655.
(12) Ding, J.; Li, J.; Sun, C.; Jiang, F.; Ju, P.; Qu, L.; Zheng, Y.; He, C. Detection of microplastics in local marine organisms using a multi-technology system. *Anal. Methods* **2019**, *11*, 78−87.
(13) Desforges, J. P. W.; Galbraith, M.; Ross, P. S. Ingestion of Microplastics by Zooplankton in the Northeast Pacific Ocean. *Arch. Environ. Contam. Toxicol.* **2015**, *69*, 320−330.
(14) Mason, V. G.; Skov, M. W.; Hiddink, J. G.; Walton, M. Microplastics alter multiple biological processes of marine benthic fauna. *Sci. Total Environ.* **2022**, *845*, 157362.
(15) Cole, M.; Lindeque, P.; Fileman, E.; Halsband, C.; Galloway, T. S. The Impact of Polystyrene Microplastics on Feeding, Function and Fecundity in the Marine Copepod Calanus helgolandicus. *Environ. Sci. Technol.* **2015**, *49*, 1130−1137.
(16) Jandang, S.; Alfonso, M. B.; Nakano, H.; Phinchan, N.; Darumas, U.; Viyakarn, V.; Chavanich, S.; Isobe, A. Possible sink of missing ocean plastic: Accumulation patterns in reef-building corals in the Gulf of Thailand. *Sci. Total Environ.* **2024**, *954*, 176210.
(17) Ding, J.; Jiang, F.; Li, J.; Wang, Z.; Sun, C.; Wang, Z.; Fu, L.; Ding, N. X.; He, C. Microplastics in the coral reef systems from Xisha Islands of South China Sea. *Environ. Sci. Technol.* **2019**, *53*, 8036−8046.
(18) Martin, C.; Corona, E.; Mahadik, G. A.; Duarte, C. M. Adhesion to coral surface as a potential sink for marine microplastics. *Environ. Pollut.* **2019**, *255*, 113281.
(19) Hall, N. M.; Berry, K. L.; Rintoul, L.; Hoogenboom, M. O. Microplastic ingestion by scleractinian corals. *Marine Biology.* **2015**, *162*, 725−732.
(20) Hierl, F.; Wu, H. C.; Westphal, H. Scleractinian corals incorporate microplastic particles: Identification from a laboratory study. *Environ. Sci. Pollut. Res. Int.* **2021**, *28*, 37882−37893.
(21) Reichert, J.; Schellenberg, J.; Schubert, P.; Wilke, T. Responses of reef building corals to microplastic exposure. *Environ. Pollut.* **2018**, *237*, 955−960.
(22) Hankins, C.; Duffy, A.; Drisco, K. Scleractinian coral microplastic ingestion: Potential calcification effects, size limits, and retention. *Mar. Pollut. Bull.* **2018**, *135*, 587−593.
(23) Allen, A. S.; Seymour, A. C.; Rittschof, D. Chemoreception drives plastic consumption in a hard coral. *Mar. Pollut. Bull.* **2017**, *124*, 198−205.
(24) Huang, W.; Chen, M.; Song, B.; Deng, J.; Shen, M.; Chen, Q.; Zeng, G.; Liang, J. Microplastics in the coral reefs and their potential impacts on corals: A mini-review. *Sci. Total Environ.* **2021**, *762*, 143112.
(25) Okubo, N.; Takahashi, S.; Nakano, Y. Microplastics disturb the anthozoan-algae symbiotic relationship. *Mar. Pollut. Bull.* **2018**, *135*, 83−89.
(26) Okubo, N.; Tamura-Nakano, M.; Watanabe, T. Experimental observation of microplastics invading the endoderm of anthozoan polyps. *Mar. Environ. Res.* **2020**, *162*, 105125.
(27) Krishnakumar, S.; Anbalagan, S.; Hussain, S.; Bharani, R.; Godson, P. S.; Srinivasalu, S. Coral annual growth band impregnated microplastics (Porites sp.): A first investigation report. *Wetl. Ecol. Manag.* **2021**, *29*, 677−687.
(28) Kniese, J.; Ritschar, S.; Bünger, L.; Feldhaar, H.; Laforsch, C.; Römpp, A.; Schmidt, H. Localisation and identification of polystyrene particles in tissue sections using Raman spectroscopic imaging. *NanoImpact* **2023**, *30*, 100465.
(29) Ribeiro-Claro, P.; Nolasco, M. M.; Araújo, C.Characterization of microplastics by Raman spectroscopy*Comprehensive Analytical Chemistry*Elsevier201775119−151
(30) Xu, J. L.; Thomas, K. V.; Luo, Z.; Gowen, A. A. FTIR and Raman imaging for microplastics analysis: State of the art, challenges and prospects. *TrAC - Trends Anal. Chem.* **2019**, *119*, 115629.
(31) Anger, P. M.; von der Esch, E.; Baumann, T.; Elsner, M.; Niessner, R.; Ivleva, N. P. Raman microspectroscopy as a tool for microplastic particle analysis. *TrAC - Trends Anal. Chem.* **2018**, *109*, 214−226.
(32) Chen, C.-F.; Ju, Y.-R.; Wang, M.-H.; Lim, Y. C.; Chen, C.-W.; Cheng, Y.-R.; Dong, C.-D. Microplastic pollution in stony coral skeletons and tissues: A case study of accumulation and interrelationship in South Penghu Marine National Park, Taiwan Strait. *J. Hazard. Mater.* **2025**, *484*, 136761.
(33) Cheng, J.-X.; Xie, X. S. *Coherent Raman scattering microscopy*; CRC press, 2016; p 610.
(34) Standish, C. D.; Trend, J.; Kleboe, J.; Chalk, T. B.; Mahajan, S.; Milton, J. A.; Page, T. M.; Robinson, L. F.; Stewart, J. A.; Foster, G. L. Correlative geochemical imaging of Desmophyllum dianthus reveals biomineralisation strategy as a key coral vital effect. *Sci. Rep.* **2024**, *14*, 11121.
(35) Cheng, J.-X.; Xie, X. S. Coherent anti-Stokes Raman scattering microscopy: Instrumentation, theory, and applications. *J. Phys. Chem. B* **2004**, *108*, 827−840.
(36) Schymanski, D.; Goldbeck, C.; Humpf, H. U.; Fürst, P. Analysis of microplastics in water by micro-Raman spectroscopy: Release of plastic particles from different packaging into mineral water. *Water Res.* **2018**, *129*, 154−162.
(37) Cabernard, L.; Roscher, L.; Lorenz, C.; Gerdts, G.; Primpke, S. Comparison of Raman and Fourier Transform infrared spectroscopy for the quantification of microplastics in the aquatic environment. *Environ. Sci. Technol.* **2018**, *52*, 13279−13288.
(38) Moura, C. C.; Tare, R. S.; Oreffo, R. O. C.; Mahajan, S. Raman spectroscopy and coherent anti- Stokes Raman scattering imaging: Prospective tools for monitoring skeletal cells and skeletal regeneration. *J. R. Soc. Interface* **2016**, *13*, 9−11.
(39) Moura, C. C.; Bourdakos, K. N.; Tare, R. S.; Oreffo, R. O. C.; Mahajan, S. Live-imaging of bioengineered cartilage tissue using multimodal non-linear molecular imaging. *Sci. Rep.* **2019**, *9*, 5561.
(40) Patel, I. I.; Steuwe, C.; Reichelt, S.; Mahajan, S. Coherent anti-Stokes Raman scattering for label-free biomedical imaging. *J. Opt.* **2013**, *15*, 094006.
(41) Chen, X.; Grégoire, S.; Formanek, F.; Galey, J.-B.; Rigneault, H. Quantitative 3D molecular cutaneous absorption in human skin using label free nonlinear microscopy. *J. Controlled Release* **2015**, *200*, 78−86.
(42) Jung, Y.; Tam, J.; Jalian, H. R.; Anderson, R. R.; Evans, C. L. Longitudinal, 3D in vivo imaging of sebaceous glands by coherent anti-stokes Raman scattering microscopy: Normal function and response to cryotherapy. *J. Invest. Dermatol.* **2015**, *135*, 39−44.
(43) Zada, L.; Leslie, H. A.; Vethaak, A. D.; Tinnevelt, G. H.; Jansen, J. J.; de Boer, J. F.; Ariese, F. Fast microplastics identification with stimulated Raman scattering microscopy. *J. Raman Spectrosc.* **2018**, *49*, 1136−1144.
(44) Takahashi, T.; Herdzik, K. P.; Bourdakos, K. N.; Read, J. A.; Mahajan, S. Selective imaging of microplastic and organic particles in flow by multimodal coherent anti-Stokes Raman scattering and two-photon excited autofluorescence analysis. *Anal. Chem.* **2021**, *93*, 5234−5240.
(45) Cole, M.; Lindeque, P.; Fileman, E.; Halsband, C.; Goodhead, R.; Moger, J.; Galloway, T. S. Microplastics ingestion by zooplankton. *Environ. Sci. Technol.* **2013**, *47*, 6646.
(46) Dullo, W.-C. Coral growth and reef growth: A brief review. *Facies* **2005**, *51*, 33−48.
(47) D'angelo, C.; Wiedenmann, J. An experimental mesocosm for long-term studies of reef corals. *J. Mar. Biol. Assoc. U. K.* **2012**, *92*, 769−775.
(48) Wiedenmann, J.; D'angelo, C.; Smith, E. G.; Hunt, A. N.; Legiret, F.-E.; Postle, A. D.; Achterberg, E. P. Nutrient enrichment can increase the susceptibility of reef corals to bleaching. *Nat. Clim. Chang.* **2013**, *3*, 160−164.
(49) D'angelo, C.; Smith, E. G.; Oswald, F.; Burt, J.; Tchernov, D.; Wiedenmann, J. Locally accelerated growth is part of the innate immune response and repair mechanisms in reef-building corals as detected by green fluorescent protein (GFP)-like pigments. *Coral Reefs* **2012**, *31*, 1045−1056.

https://doi.org/10.1021/acs.est.5c10668
Environ. Sci. Technol. 2026, 60, 3438−3448

(50) Tang, J.; Ni, X.; Zhou, Z.; Wang, L.; Lin, S. Acute microplastic exposure raises stress response and suppresses detoxification and immune capacities in the scleractinian coral Pocillopora damicornis. *Environ. Pollut.* **2018**, *243*, 66−74.
(51) Su, Y.; Zhang, K.; Zhou, Z.; Wang, J.; Yang, X.; Tang, J.; Li, H.; Lin, S. Microplastic exposure represses the growth of endosymbiotic dinoflagellate Cladocopium goreaui in culture through affecting its apoptosis and metabolism. *Chemosphere* **2020**, *244*, 125485.
(52) Lee, Y. J.; Snyder, C. R.; Forster, A. M.; Cicerone, M. T.; Wu, W.-L. Imaging the molecular structure of polyethylene blends with broadband coherent Raman microscopy. *ACS Macro Lett.* **2012**, *1*, 1347−1351.
(53) Neumann-Micheau, N.; Tributsch, H. Luminescence light collection technology in the aragonite of stone corals. *Bioinspir. Biomim.* **2018**, *13*, 066006.
(54) Takahashi, T.; Liu, Z.; Thevar, T.; Burns, N.; Mahajan, S.; Lindsay, D.; Watson, J.; Thornton, B. Identification of microplastics in a large water volume by integrated holography and Raman spectroscopy. *Appl. Opt.* **2020**, *59*, 5073−5078.
(55) Buckingham, M.; D'angelo, C.; Chalk, T.; Foster, G.; Johnson, K.; Connelly, Z.; Olla, C.; Saeed, M.; Wiedenmann, J. Impact of nitrogen (N) and phosphorus (P) enrichment and skewed N: P stoichiometry on the skeletal formation and microstructure of symbiotic reef corals. *Coral Reefs* **2022**, *41*, 1147−1159.
(56) Hashimoto, K.; Omachi, J.; Ideguchi, T. Ultra-broadband rapid-scan Fourier-transform CARS spectroscopy with sub-10-fs optical pulses. *Optics Express.* **2018**, *26*, 14307−14314.
(57) Nishiyama, R.; Furuya, K.; Tamura, T.; Nakao, R.; Peterson, W.; Hiramatsu, K.; Ding, T.; Goda, K. Fourier Transform Coherent Anti-Stokes Raman Scattering Spectroscopy: A Comprehensive Review. *Anal. Chem.* **2024**, *96*, 18322−18336.
(58) Phan, S.; Padilla-Gamiño, J. L.; Luscombe, C. K. The effect of weathering environments on microplastic chemical identification with Raman and IR spectroscopy: Part I. polyethylene and polypropylene. *Polym. Test.* **2022**, *116*, 107752.
(59) Hiejima, Y.; Kida, T.; Takeda, K.; Igarashi, T.; Nitta, K.-H. Microscopic structural changes during photodegradation of low-density polyethylene detected by Raman spectroscopy. *Polym. Degrad. Stab.* **2018**, *150*, 67−72.
(60) Brown, B. Coral bleaching: Causes and consequences. *Coral Reefs* **1997**, *16*, S129−S138.
(61) Shapiro, O. H.; Kramarsky-Winter, E.; Gavish, A. R.; Stocker, R.; Vardi, A. A coral-on-a-chip microfluidic platform enabling live-imaging microscopy of reef-building corals. *Nat. Commun.* **2016**, *7*, 10860.
(62) La Jeunesse, T. C. Zooxanthellae. *Curr. Biol.* **2020**, *30*, R1110−R1113.
(63) Liu, Y.; Wu, H.; Shu, Y.; Hua, Y.; Fu, P. Symbiodiniaceae and Ruegeria sp. co-cultivation to enhance nutrient exchanges in coral holobiont. *Microorganisms* **2024**, *12*, 1217.
(64) Isa, V.; Seveso, D.; Diamante, L.; Montalbetti, E.; Montano, S.; Gobbato, J.; Lavorano, S.; Galli, P.; Louis, Y. D. Physical and cellular impact of environmentally relevant microplastic exposure on thermally challenged Pocillopora damicornis (Cnidaria, Scleractinia). *Sci. Total Environ.* **2024**, *918*, 170651.

https://doi.org/10.1021/acs.est.5c10668
Environ. Sci. Technol. 2026, 60, 3438−3448